Manganese abundances in mercury–manganese stars

C. M. Jomaron, M. M. Dworetsky[★] and C. S. Allen

Department of Physics and Astronomy, University College London, London WC1E 6BT

ABSTRACT

We use exact curve-of-growth analysis and spectral synthesis to deduce the abundance of Mn from high signal-to-noise ratio visible-region echelle spectra of selected Mn I and Mn II lines in 24 HgMn stars. The results are compared with the Mn abundances derived from UV resonance lines by Smith & Dworetsky. We find excellent agreement for several unblended Mn lines and confirm the temperature dependence of the Mn abundance found by Smith & Dworetsky. The Mn II lines at $\lambda\lambda 4206$ and 4326 are much stronger than one would predict from the mean Mn abundances. The lack of agreement is greatest for stars with the strongest Mn II lines. Using ad hoc multicomponent fits to the profiles of sharp-lined stars, we show that most of the discrepancies can be explained by hyperfine structure that desaturates the lines, with full widths of the order of 0.06–0.09 Å.

Key words: line: profiles – stars: abundances – stars: chemically peculiar.

1 INTRODUCTION

HgMn stars are a subclass of chemically peculiar star occupying the spectral region $\sim$ A0/B9–B6 (10 500–16 000 K). Observationally, these stars are characterized by extremely low rotational velocities, weak or non-detectable magnetic fields and photometric variability, and atmospheric deficiencies of light elements (e.g. He, Al, N) coupled with enhancements of the heavy elements (e.g. Hg, Mn, Pt, Sr, Ga). In addition, the heavy elements also have non-terrestrial isotopic abundances (Smith 1997; Bohlender, Dworetsky & Jomaron 1998). The currently favoured mechanism for explaining these anomalies is the radiative diffusion hypothesis (Michaud 1970). This work has been advanced in the form of a parameter-free model (Michaud 1986).

The quiescent atmospheres of these stars make them one of the best natural laboratories for studying the competing processes of gravitational diffusion and radiative levitation (Vauclair & Vauclair 1982). In the absence of disrupting mechanisms such as convection, rotationally induced meridional currents, high microturbulence and magnetic fields, certain elements reach a factor of 10^5 enhancement over their cosmic abundance. Because of the strength and sharpness of normally exotic spectroscopic lines, HgMn stars are also useful for constraining fundamental atomic data (Lanz 1995).

The study of UV resonance lines of manganese by Smith & Dworetsky (1993, hereafter SD93) showed that the Mn abundances were not only greatly enhanced over the solar value, but also correlated with T_{eff}. Their work confirmed and extended previous studies that had drawn attention to this correlation, in particular Aller (1970), Heacox (1979) and Adelman (1989). Their data also confirmed the existence of a small class of hot, but only mildly

enhanced Mn stars (Cowley 1980), with 46 Aql as its exemplar (Smith 1993). In the hottest stars it was also found that there was great difficulty in fitting the wings of the resonance lines simultaneously with the cores, the latter being deeper than expected for local thermodynamic equilibrium (LTE) formation. However, the abundances were consistent with the detailed calculations of Alecian & Michaud (1981). SD93 speculated on the presence of vertical abundance gradients of Mn within the atmosphere (i.e. stratification), but the evidence was insufficient to conclude one way or the other.

In this paper, we present an abundance analysis of visible Mn I and Mn II lines using both spectral synthesis (i.e. line profile fitting methods) and exact curve of growth (equivalent width matching). These analyses, performed under the assumption of LTE, agree closely with, and confirm in detail, the abundances of Mn found by SD93 from resonance lines measured in *IUE* spectra. The only differences were for double-lined binary stars where SD93 made no allowance for dilution or blending effects. The use here (Section 3.1) of model atmospheres with improved blanketing has only a small effect on the results.

Abt (1952) and Booth & Blackwell (1983) demonstrated that hyperfine structure (hfs) can have severe effects on abundance calculations of Mn I if it is not properly taken into account. Although their particular interests were F and G stars and the solar spectrum, Booth & Blackwell's estimates for hotter stars indicated that abundance errors of more than 1 dex could be made by ignoring hfs. In this paper, we consider hfs models for Mn II lines similar to those discussed for Mn I by Booth & Blackwell. Adelman (1992) suggested that the neglect of hfs in his analysis produced spurious microturbulent velocities ξ deduced from Mn II in HgMn stars; we note that he also omitted the lines $\lambda\lambda 4206$ and 4326 in analyses of stars with high Mn

[★]Guest Observer, Lick Observatory.

Table 1. Stellar parameters. Microturbulent velocity ξ and projected equatorial rotational velocity $v \sin i$ in km s^{-1}.

Star	HD	T_{eff} (K)	$\log g$ (cm s^{-2})	ξ	$v \sin i$
87 Psc	7374	13 150	4.00	1.5	21.0
ϕ Phe	11753	10 700	3.80	0.5	13.0
53 Tau	27295	12 000	4.25	0.0	6.5
μ Lep	33904	12 800	3.85	0.0	15.5
HR 1800[a]	35548	11 050	3.80	0.5	3.0
33 Gem	49606	14 400	3.85	0.5	22.0
HR 2676	53929	14 050	3.60	1.0	25.0
HR 2844	58661	13 460	3.80	0.5	27.0
ν Cnc	77350	10 400	3.60	0.1	13.0
κ Cnc	78316	13 500	3.80	0.0	7.0
HR 4072[a]	89822	10 500	3.95	1.1	2.0
χ Lup[a]	141556	10 750	4.00	1.0	2.0
ι CrB[a]	143807	11 000	4.00	0.2	5.0
υ Her	144206	12 000	3.80	0.6	9.0
ϕ Her	145389	11 650	4.00	0.4	10.1
28 Her	149121	11 000	3.80	0.0	10.0
HR 6997	172044	14 500	3.90	1.5	36.0
112 Her[a]	174933	13 100	4.10	0.0	5.5
HR 7143	175640	12 100	4.00	1.0	2.0
HR 7361	182308	13 650	3.55	0.0	8.2
46 Aql	186122	13 000	3.65	0.0	3.0
HR 7664	190229	13 200	3.60	0.8	8.0
HR 7775	193452	10 800	3.95	0.0	0.0
β Scl	221507	12 400	3.90	0.0	25.0

[a]Binaries with two spectra (parameters refer to the primary). Explicit allowances for dilution effects are discussed in the text.

anomalies. Although there are no extant laboratory data for Mn II in the literature at the time of writing this paper, we are able to show that some Mn II lines must have hfs structures 0.06–0.09 Å wide, and that it is the most likely explanation for anomalous strengths of $\lambda\lambda 4206$ and 4326.

2 OBSERVATIONS

Our stellar sample is based upon that of SD93, who analysed *IUE* data on the UV resonance lines of 26 HgMn, four superficially normal and 10 normal stars. We observed 24 of the HgMn stars in the SD93 sample. The two excluded stars are 36 Lyn (which had been misclassified as an HgMn star) and HR 6000 (which was not observed). The physical parameters of the 24 stars are given in Table 1.

Five stars are noted as double-lined spectroscopic binaries in Table 1; one of these (HR 1800) is better described as a close visual binary in which we can see evidence of the secondary spectrum as rotationally broadened features. The parameters quoted in all five cases are those adopted for the primary star. The adopted light ratios (L_A/L_B) at $\lambda 4520$ are from Harman (1997): HR 4072, 5.45; χ Lup, 3.65; ι CrB, 2.70; or from Ryabchikova, Zakhorova & Adelman (1996): 112 Her, 6.3 from their table 2. Suitable adjustments for other wavelength regions were made. The adopted light ratio for the visual binary HR 1800 ($\rho = 0.243$ arcsec) is 2.45, based on $\Delta H_p = 0.96$ mag from *The Hipparcos Catalogue* (ESA 1997). Another star, 33 Gem, is suspected of being double-lined but there is not yet any information on the orbit or light ratio (Hubrig & Launhardt 1993); we treat it as a single star or 'average component'. We note that Adelman, Philip & Adelman (1996)

also treated 33 Gem as a single star, noting that the question of binarity could not be conclusively resolved with their data.

Northern Hemisphere observations were taken with the Hamilton Echelle Spectrograph (HES) – Vogt (1987) – at Lick Observatory, fed by the 0.6-m Coudé Auxilliary Telescope (CAT), during four runs in 1994–97. Further details of the instrument can be found in Misch (1997). Stars south of $-35°$ were acquired as service observations at the Anglo-Australian Telescope (AAT) using the UCL Echelle spectrograph. Shortly before our observations in 1994, some of the HES optical components were replaced, improving the resolution and instrumental profile, and making it possible to use the full field of the 2048×2048 CCDs to maximum advantage. We used both the unthinned phosphor-coated Orbit CCD (Dewar 13) and, from 1995 July, the thinned Ford CCD (Dewar 6), depending on availability as the latter is shared with the multi-object spectrograph on the 3-m telescope. The spectral range for the observations was 3800–9000 Å, except for the AAT data which were only obtained in the range 3700–4700 Å, with the TEK2 CCD. Typical signal-to-noise ratios (*S/N*) per pixel in the centres of orders ranged from 75 to 250. The Orbit CCD is cosmetically very clean, with very few bad pixels or columns, while the thinned Ford CCD contains several column defects but offers a much higher detector quantum efficiency in the blue. We used the Ford CCD whenever it was available. With the slit settings used, the combination of spectrographs and CCDs gave resolutions of $R \approx 46\,500$ for the HES and $R \approx 44\,000$ for the UCLES. Flat-fields were made using polar axis quartz lamps and wavelength calibrations were obtained with Th–Ar comparisons.

The echelle spectra were extracted and calibrated using standard IRAF extraction packages (Valdes 1990; Churchill 1995), running on UCL's Starlink node. Previous measurements (Allen 1998) showed that there were no measurable effects of parasitic light (residual scattered light) in the line profiles provided that general scattered light in the adjacent interorder spaces was taken as the subtracted background. In practice the residual scattered light was less than *c.* 1 per cent; we have therefore made no corrections to account for it. Allen's method is based on a direct comparison of the solar spectrum (as reflected from the roof of the CAT coelostat) observed with the HES, with the Kitt Peak Solar Flux Atlas (Kurucz et al. 1984). As the latter was obtained using a Fourier transform spectrometer, it has no measurable parasitic light. The KPNO spectrum is convolved with a suitable instrumental profile to match the HES data; both spectra must be normalized at the same points for a valid comparison. The ratio of summed equivalent widths of various features with good adjacent continuum points, in many different spectral orders, provides the measure of the amount of parasitic light.

3 ABUNDANCE DETERMINATION

3.1 Stellar parameters, stellar atmospheres, atomic data and line selection

Abundances were determined using the exact curve-of-growth technique. For this method, we measured the equivalent widths, W_λ, of Mn absorption lines in the programme spectra and compared these values with the calculated curves of growth for each line, which were generated (assuming LTE) by our spectral synthesis code UCLSYN (Smith & Dworetsky 1988; Smith 1992). The necessary atmospheric parameters given in Table 1 – T_{eff}, $\log g$ and microturbulence (ξ) – were taken from SD93, except for 112 Her where we used the values given by Ryabchikova et al. (1996). The

Table 2. Mn equivalent widths and abundances in the HgMn programme stars. $\log A(\mathrm{H}) = 12$.

Star	Mn II								Mn I				mean	Pub.
	λ4478.637		λ4365.220		λ4363.255		λ3917.318		λ4030.753		λ4034.483		$\log A_\star \pm$ s.d.	UV
	W_λ	$\log A$	W_λ	$\log A$	W_λ	$\log A$	W_λ	$\log A$	W_λ	$\log A$	W_λ	$\log A$		
87 Psc	46.5	7.29	27.0	7.25	28.0	7.40	29.0	7.24	—	—	—	—	7.30± 0.07	7.40
φ Phe	11.5	6.06	—	—	5.0	6.10	9.5	6.28	15.0	6.13	—	—	6.14± 0.10	6.20
53 Tau	44.0	7.21	30.0	7.28	24.0	7.22	31.5	7.30	36.5	7.46	20.0	7.32	7.30± 0.09	7.25
μ Lep	52.0	7.53	38.5	7.56	35.5	7.62	38.0	7.54	18.0	7.57	14.0	7.76	7.60± 0.09	7.50
HR 1800[a]	31.0	6.72	20.0	6.80	18.0	6.81	20.0	6.74	28.0	6.77	20.0	6.88	6.79± 0.06	6.05
33 Gem	42.0	7.59	30.0	7.66	23.0	7.61	—	—	—	—	—	—	7.62± 0.04	7.50
HR 2676	5.0	6.16	—	—	—	—	—	—	—	—	—	—	6.16	6.15
HR 2844	67.0	8.04	47.5	7.93	47.0	8.09	45.0	7.87	—	—	—	—	7.98± 0.10	7.90
ν Cnc	—	—	—	—	—	—	—	—	—	—	—	—	<6.30	6.00
κ Cnc	50.0	7.63	35.0	7.61	33.0	7.70	33.0	7.52	—	—	—	—	7.62± 0.07	7.80
HR 4072[a]	15.5	6.24	9.5	6.38	8.0	6.35	—	—	17.5	6.00	—	—	6.24± 0.17	5.90
χ Lup[a]	5.0	5.69	—	—	—	—	—	—	7.5	5.73	—	—	5.71	4.85
ι CrB[a]	33.5	6.83	20.0	6.86	17.0	6.83	17.5	6.71	32.0	6.79	17.0	6.69	6.79± 0.07	6.55
υ Her	41.5	7.08	27.0	7.09	26.0	7.16	27.0	7.05	14.0	6.93	12.0	7.19	7.08± 0.09	7.10
φ Her	32.5	6.85	19.0	6.86	18.0	6.92	19.0	6.80	27.0	7.06	13.5	6.96	6.91± 0.09	6.95
28 Her	15.5	6.26	8.0	6.29	—	—	7.5	6.19	—	—	—	—	6.25± 0.05	6.35
HR 6997	51.0	7.70	43.0	7.91	38.0	7.96	44.0	7.89	—	—	—	—	7.87± 0.11	8.15
112 Her[a]	20.0	6.71	9.5	6.68	9.5	6.80	13.0	6.76	—	—	—	—	6.74± 0.06	6.75
HR 7143	55.0	7.38	40.5	7.45	37.5	7.50	43.5	7.52	41.0	7.65	23.0	7.54	7.51± 0.09	7.65
HR 7361	58.5	7.94	47.0	8.00	43.0	8.05	47.0	8.02	15.5	8.18	7.0	8.10	8.05± 0.08	7.90
46 Aql	6.0	6.02	5.0	6.31	4.0	6.32	4.0	6.14	—	—	—	—	6.20± 0.14	6.30
HR 7664	11.5	6.39	6.5	6.48	6.0	6.56	5.5	6.33	—	—	—	—	6.44± 0.10	6.30
HR 7775	9.0	5.98	4.0	5.99	4.5	6.10	—	—	12.5	6.06	5.0	5.94	6.01± 0.06	6.15
β Scl	51.5	7.44	38.0	7.49	36.0	7.56	39.0	7.51	—	—	—	—	7.50± 0.05	7.40
$\overline{\log(A/A_\star)}$		−0.05		0.00		+0.05		−0.04		+0.02		+0.04		
$\log gf$		−0.95		−1.35		−1.91		−1.15		−0.47		−0.81		

[a]Binaries with two spectra. The W_λ values are corrected for dilution effects.

values of $v \sin i$ are taken from Dworetsky, Jomaron & Smith (1998). In the cases of the five binaries with double spectra, we adopted the light ratios cited in Section 2 in order to correct for dilution effects using the BINSYN code (Smalley, private communication), an extension of UCLSYN. We used a combined grid of ATLAS9 model atmospheres: the 2 km s^{-1} grid of Kurucz (1993), and the COLK95 grid of Castelli, Gratton & Kurucz (1997) for cooler stars, interpolating to produce a model at the chosen T_{eff} and $\log g$ of each star.

There appear to be no other published data on laboratory oscillator strengths for visible-region Mn II lines except for Warner (1967a). We adopt the calculations of Kurucz (1990) taken from CD23. If we adjust the Warner $\log gf$-values by the prescription of Smith (1976), we find that the Kurucz calculations tend to give values of c. 0.4 dex smaller for our lines from higher excitation levels. It is not possible to use one set of data to 'check' the other; a modern set of measured absolute oscillator strengths for Mn II would be required. For the Mn I lines, we adopt the oscillator strengths of Martin, Fuhr & Wiese (1988), which are the same as those given in CD23. For both neutral and ionized Mn we adopt the ratio of radiative to classical damping parameters, Γ_R/Γ_{cl}, given by Kurucz but use the internal algorithms of UCLSYN to estimate the Stark damping parameter Γ_S for each line. Van der Waals contributions to line broadening are expected to be small; a suitable approximation by Warner (1967b) is used.

Rather than measuring many tens of lines, of which some may be partially blended or have poorly known gf-values, relying on statistical averaging to give a valid result which may none the less be biased, and fully synthesizing the profiles of many lines to mitigate the blending problem, the approach followed here was to find a small sample of Mn lines, all of which could be shown to be unblended over a wide range of T_{eff} and composition. A search for such lines was carried out by Allen (1998). The following lines were selected as being appropriate for a high-accuracy curve-of-growth analysis: Mn II λλ4478, 4365, 4363, 4326, 4206, 3917; Mn I λλ4030 and 4034. Allen used the criteria that lines should be strong enough to appear in most HgMn stars, be blend-free and have well-determined atomic parameters. However, Allen noted that λ4206 systematically produced anomalously large abundances; the severity of the anomaly was proportional to the line strength.

3.2 Equivalent widths and abundance results

Equivalent widths (measured to the nearest 0.5 mÅ) and abundances derived from the individual Mn lines are shown in Table 2. The equivalent widths for the five binaries noted in Table 1 have been scaled to compensate for the dilution of light arising from the continuum of their secondaries. The unweighted means and standard deviations of the line abundances may be compared with the UV abundances taken from SD93. In accordance with Allen's result, it was found that Mn II λ4206 (see later) gave rise to anomalously high abundances. We also found that Mn II λ4326 followed a similar pattern of anomalously high abundances. These two lines are thus examined separately later in this paper. Examples of spectra of the remaining Mn lines can be seen in Fig. 1.
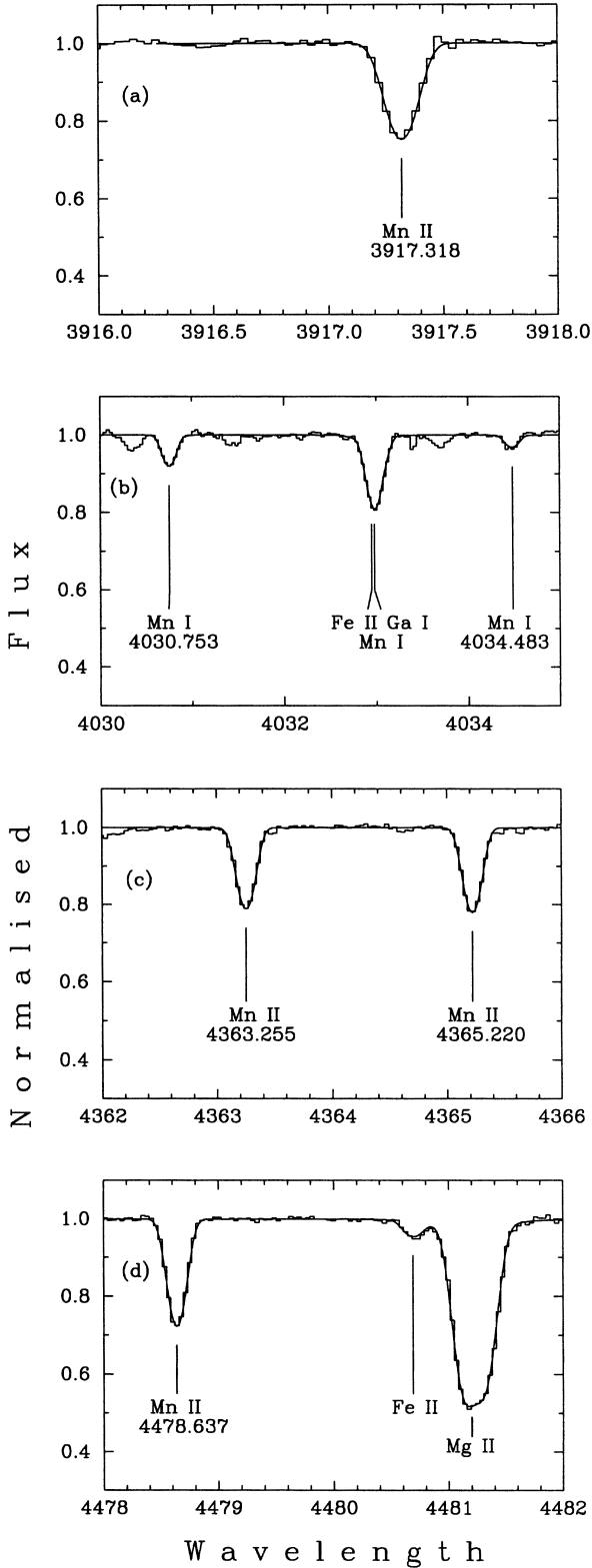
Figure 1. The six Mn lines used in this abundance analysis. These spectra are of HR 7361. Histograms represent observations; continuous lines represent synthetic spectra.

We were unable to measure with certainty any of the lines in Table 2 for the SD93 normal or superficially normal comparison stars. This result is consistent with them having the cosmic abundance of Mn, $\log A = 5.39$ (Anders & Grevesse 1989).

3.3 Errors

The external errors on the mean abundances are obtained by propagating the uncertainties owing to the measured W_λ, the atomic parameters and the stellar T_{eff} (which affects the ionization balance), assuming they are independent of one another. Following the SD93 convention, we have adopted estimates of the errors on each parameter as follows: ± 0.25 dex in $\log g$, ± 250 K in T_{eff}, ± 50 per cent in the Stark damping (Γ_S), ± 0.5 km s^{-1} in the microturbulence (ξ) and ± 5 per cent in W_λ. Propagating these errors through the curve-of-growth analysis for the Mn II $\lambda 4478$ line, using a model atmosphere based around $T_{\text{eff}} = 13\,000$ K, $\log g = 4.0$, $\xi = 1$, with a $+2$ dex Mn abundance enhancement over the solar value, leads to the following representative errors in the derived Mn abundances: ± 0.01 dex (Γ_S); ± 0.02 dex ($\log g$); ± 0.05 dex (T_{eff}); ± 0.06 dex (ξ); ± 0.06 dex (W_λ).

To obtain the internal error on the mean value of abundance for each star, we calculate the standard deviation of the set of measured lines (Table 2). The mean standard deviation over the entire sample is ± 0.09 dex. Remarkably, there is no significant overall difference between the mean abundances derived from the Mn I and Mn II lines, despite the fact that the T_{eff} sensitivity of Mn I is ± 0.15 dex for variations of ± 250 K. There is no evidence for systematic differences between abundances derived from the different lines in Table 2; the average deviations, $\overline{\log(A/A_\star)}$, are only a few hundredths of a dex.

Finally, we can estimate a purely 'experimental' error on the abundance determinations for individual lines by varying the abundance values used in our synthetic fits (see Section 3.4) and seeing how rapidly the synthetic profiles depart from the observed profiles. For visual fitting of synthetic profiles to the observed data, changes of $c. \pm 0.02$–0.05 dex produce a significantly degraded quality of fit, depending upon the S/N of the spectrum.

These comparisons give us confidence that the abundances we have derived are internally consistent with expected errors of observation. It is remarkable that there appears to be little significant extra scatter owing to errors in $\log gf$. Throughout this analysis we assume that Mn is homogeneously distributed with depth. Stratification of elements by diffusion and gravitational settling, and non-LTE are both possible complications which must be considered in such analyses. However, we do not maintain that the full agreement of Mn I and Mn II 'proves' that there are no stratification or non-LTE effects on the Mn I abundances compared with Mn II, only that, if any such effects are present, either they are small or the factors involved apparently cancel out over a wide range of T_{eff}. Detailed considerations of such possibilities are beyond the scope of this paper.

3.4 Comparison of curve of growth with synthesis

To validate the use of the curve-of-growth technique with such a small set of lines, the derived abundances were compared with abundances obtained via synthetic profile fits. Using UCLSYN, we synthesized spectral windows around the Mn lines in Table 2 in several of the single sample stars, selected to form a representative subsample over the abundance range. Fits of the synthetic spectra to the observations were made by eye. Table 3 shows the differences between the abundances derived using the two methods, and Fig. 1 shows representative synthetic fits to the Mn lines in HR 7361.

The Mn I lines at $\lambda\lambda 4030$ and 4034, and Mn II lines at $\lambda\lambda 4478$, 4365, 4363 and 3917 were all well fitted by the synthetic profiles, and contain known blends contributing no more than 2–3 per cent

Table 3. Differences between abundances derived using spectral synthesis and exact curve of growth.

Star	Mean log A(Mn)	Mn II (synth − COG)				Mn I (synth − COG)		Mean
		λ4478	λ4365	λ4363	λ3917	λ4030	λ4034	
HR 7775	6.01	−0.03	−0.09	−0.15	—	−0.01	0.06	−0.04
28 Her	6.25	−0.01	−0.09	—	−0.04	—	—	−0.05
υ Her	7.08	0.05	0.02	0.00	−0.01	0.22	−0.04	0.04
HR 7143	7.51	0.07	0.10	−0.05	−0.07	0.00	0.01	0.01
HR 7361	8.05	−0.09	0.00	0.00	−0.12	−0.06	+0.05	−0.04
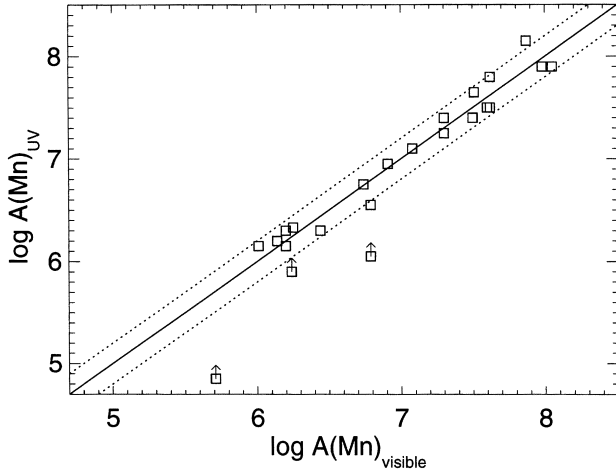
Figure 2. Mn abundances from visible and UV spectra. The solid line is that of equality. The dotted lines indicate a ± 0.2 dex deviation from equality. All three stars substantially exceeding these limits are binary systems (shown with arrows).

of the total W_λ over our entire range of T_{eff} and composition. Neither Mn II λ4206 nor λ4326 could be fitted with single line profiles with parameters similar to the other Mn lines. In most cases, no fit could be obtained where the wings and core of the line were fitted simultaneously. This effect is similar to that seen in Ga II, which recent work by Dworetsky et al. (1998) demonstrated is due to hyperfine structure. These two lines were thus excluded from the abundance analysis and we shall return to them later.

For our final selection of six Mn lines, there would appear to be no significant systematic difference between the abundances derived by the profile and curve-of-growth techniques; the mean difference is only −0.04 dex, somewhat smaller than the mean standard deviation on the abundances derived from our curve-of-growth analysis on the six Mn lines (0.09 dex). We conclude that the curve-of-growth technique is sufficiently accurate, when using a carefully selected set of lines, to reproduce results from the more time-consuming spectral synthesis method.

4 COMPARISON WITH UV DATA

Fig. 2 shows our visible-region mean abundances versus the SD93 UV-region abundances. The stars exhibit a very good match between the UV abundances and our visible-region abundances, with an apparently random scatter of the order of 0.1–0.2 dex. Only three stars show larger discrepancies, all of which are binary systems in which the spectra of both components are visible.

We note that SD93 made no allowance for binarity in their

results, on the assumption that the UV flux of the secondary would be unimportant, except for a few rare cases (they cite HR 1800, HR 4072, ι CrB and χ Lup as being possible exceptions). In the current visible-region study, we have accounted for dilution by scaling the observed W_λ for the Mn lines in accordance with the light ratio deduced for each binary system (see Section 2).

If binarity were ignored, the true strength of the Mn lines would be underestimated and thus the derived abundance would be too low. Indeed this is exactly what we find for the UV results when compared with visible-region results. The worst offender is the double-lined binary χ Lup. In this system the UV lines should be significantly diluted by the companion star, leading to an underestimate of the UV Mn abundance, exactly as found. The other stars showing larger discrepancies from our mean results (HR 1800, ι CrB, HR 4072) are double-lined binaries, and show greater Mn abundances in the visible than in the UV, again as expected. The other binary systems appear to have negligible UV contribution from the secondary star and their treatment as single by SD93 would appear justified in that context.

5 MN II λλ4206 AND 4326

The expected equivalent widths of Mn II λλ4206 and 4326 were calculated for each star, based on the mean Mn abundance derived from the other visible-region Mn II lines. For this calculation, we have made the usual assumption that the lines have only one component. The measured equivalent widths are compared with the calculated values in Table 4 (dilution effects in the binaries have been taken into account by scaling up the observed values). Fig. 3 demonstrates the discrepancy between the predicted strengths of both lines and their observed strengths, which tends to get worse at high abundances; stars with low abundances do not show this disagreement. From Fig. 4, it is clear that this discrepancy is more directly related to the strength of the lines than to the total atmospheric abundance of Mn.

Attempts to account for these anomalies by adjustments in atomic line parameters (log gf, Γ_R, Γ_S) or in stellar parameters (ξ) proved unfruitful. Further investigation revealed that the λλ4206 and 4326 features in the narrow-line star HR 7775 (Figs 5 and 6) were visibly broader than the other lines of Mn II. (Note that, for the work presented here, we did not make a detailed search for other Mn II lines with visible broadening or curve-of-growth anomalies, either of which could indicate strong hfs effects. A further search for lines that may show similar effects is the subject of future investigations.)

The most obvious candidate for a physical cause is hyperfine structure. We were unable to find any literature describing measured or theoretical hfs in these lines, but the behaviour observed in Figs 3–8 appears consistent with the hypothesis that their profiles are significantly affected by hfs: in weak-lined stars where the

Table 4. Mn II λλ4206 and 4326. The calculated values of W_λ are based on the assumption of single-component line structures and are clearly too weak in stars with high Mn abundances. The individual line abundances are based on the adopted hfs multicomponent models in Table 5.

Star	$\log A_{\mathrm{MnII}}$	W_{4206}		$\log A_{4206}$	W_{4326}		$\log A_{4326}$
		calc	obs		calc	obs	
87 Psc	7.30	44	95	7.80	51	86	7.82
φ Phe	6.15	14	20	6.25	19	25	6.24
53 Tau	7.25	45	93	7.66	45	77	7.70
μ Lep	7.56	52	100	7.92	54	87	7.97
HR 1800	6.77	33	60	6.97	39	58	6.95
33 Gem	7.62	39	63	7.71	45	65	7.81
HR 2844	7.98	60	110	8.29	64	101	8.46
κ Cnc	7.62	46	96	8.04	51	83	8.05
HR 4072	6.32	17	30	6.52	24	31	6.41
χ Lup	5.69	5	7	5.80	7	8	5.71
ι CrB	6.81	32	64	7.06	37	49	6.86
υ Her	7.10	41	89	7.51	47	85	7.68
φ Her	6.86	34	64	7.13	37	64	7.22
28 Her	6.25	16	30	6.51	21	34	6.47
HR 6997	7.87	54	110	8.44	60	103	8.57
112 Her	6.74	19	30	6.95	25	39	6.95
HR 7143	7.46	58	115	7.96	59	97	7.97
HR 7361	8.00	58	120	8.64	62	106	8.65
46 Aql	6.20	8	9	6.23	12	11	6.10
HR 7664	6.44	11	19	6.64	18	25	6.59
HR 7775	6.02	10	10	5.96	14	14	5.98
β Scl	7.50	51	100	7.82	54	86	7.86
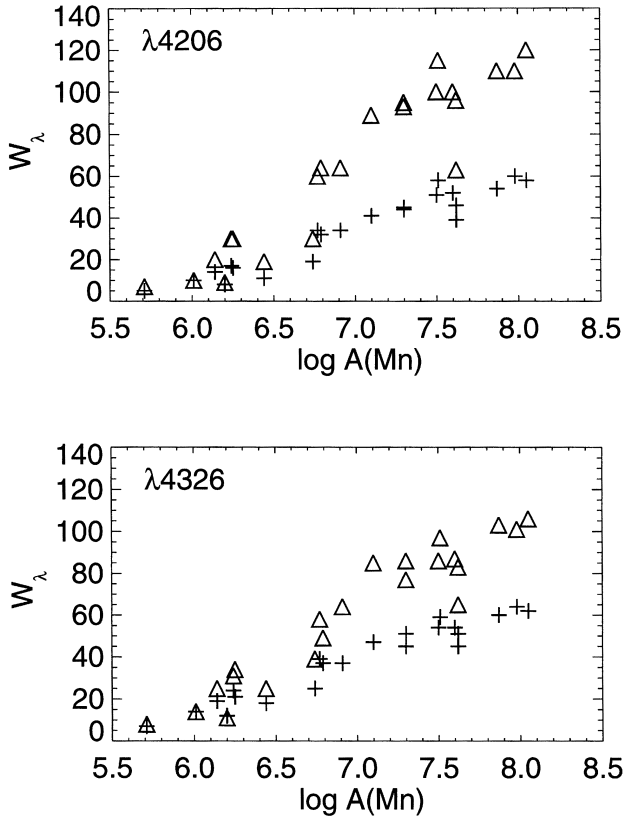
Figure 3. Mn II discrepancy in λλ4206 and 4326: calculated and observed equivalent widths are denoted by crosses and triangles, respectively.

combined feature is too weak to be saturated, the hfs will effectively spread the lines out; in strong-lined stars where the feature is saturated, the action of the hfs will be to desaturate the lines, making them stronger.

This hypothesis was tested by constructing several simplified hfs models for these lines.

For λ4206, each model contained a number of equal-strength components, spread over a wavelength range Δλ. The only constraint on Δλ was that the synthesized lines should be consistent with the width of the weak observed lines in HR 7775. We tested two- and three-component models (the total *gf* divided equally amongst the components) with the components spread over equal intervals. We found that splitting the line into three components (with $\Delta\lambda_{1-3} = 0.086$ Å; see Table 5) allows the synthetic profile to fit well, at an abundance consistent with the other lines of Mn, for nearly all stars. Example plots of the way in which introducing hfs makes a fit to the λ4206 line possible are shown for HR 7775 (Fig. 5) and HR 7361 (Fig. 7). The two-component model ($\Delta\lambda_{1-2} = 0.070$ Å) did not provide enough desaturation for the very strong-lined stars, nor did it fit HR 7775 at the line centre; we attribute lack of perfect agreement to the simplified symmetric structure adopted (normally hfs produces 'flag' patterns, with a mixture of strong and weak components). Increasing the number of components beyond three had little further effect; once there is enough hfs to make the components individually unsaturated (separated from one another by $\gtrsim 1$ thermal line width), adding in extra components broadens the line wings but does not deepen it significantly. The actual pattern should have 15 components ($I = 5/2$, $J_u = 4$, $J_1 = 5$), so it is obvious that our model is only a crude approximation.

The λ4326 line is visibly asymmetric in HR 7775 and the other stars with low $v \sin i$. After several trials, we adopted the simplified structure shown in Table 5 and Figs 6 and 8 as a compromise, in
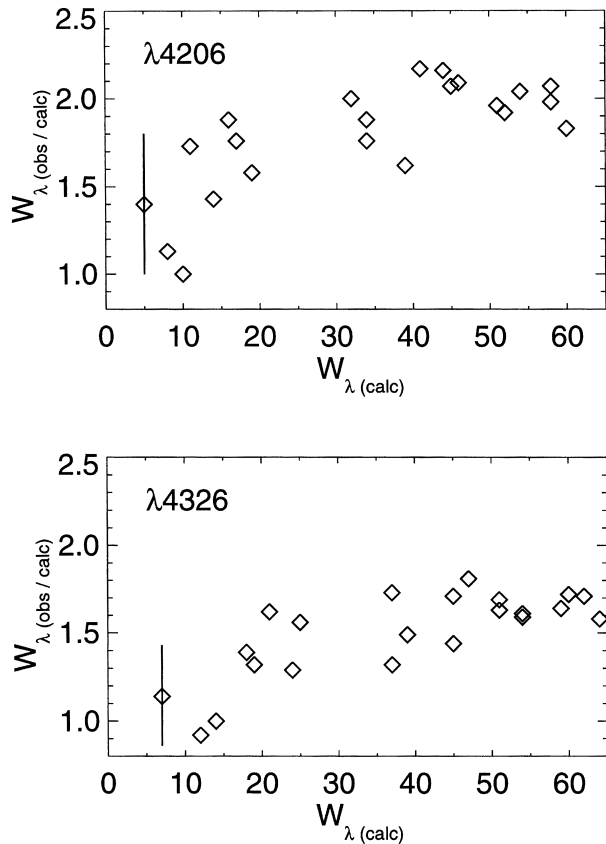
Figure 4. Mn II discrepancy in λ4206 and λλ4326: ratio (obs/calc) versus equivalent width. The calculated values represent single-component line models. The points for the weakest Mn star have considerable uncertainty and are shown with appropriately large error bars.
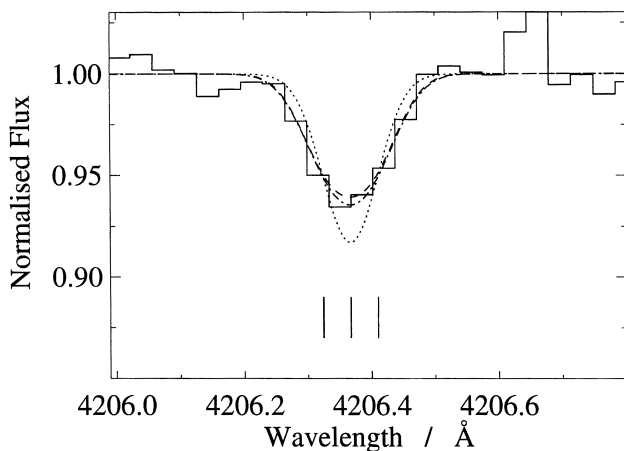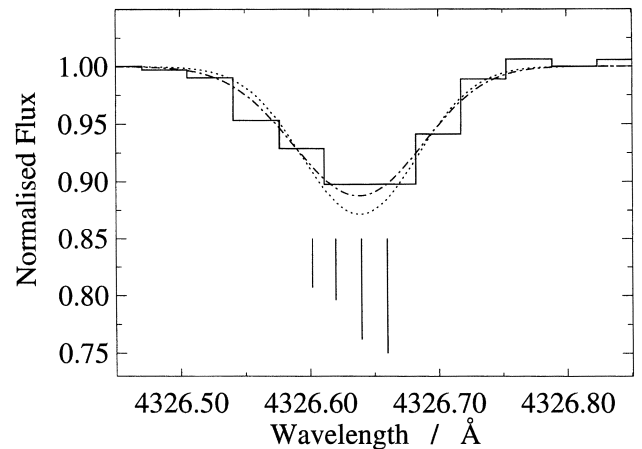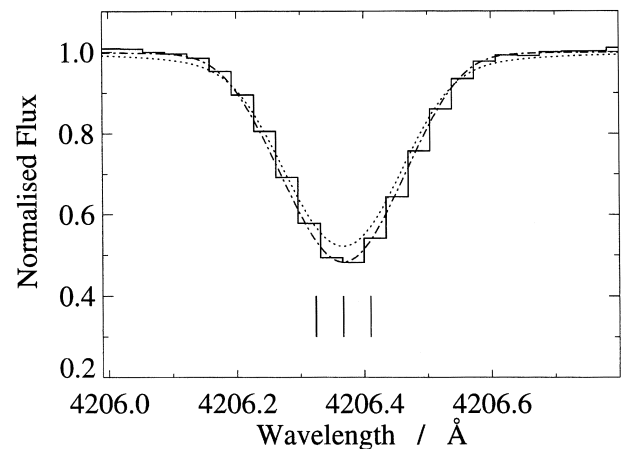

Figure 6. The Mn II λ4326 line in HR 7775 (histogram). A single-line fit (dotted line) for the observed W_λ does not match well. Using a four-component (dot–dash line) hfs model (see Table 5) provides a better fit. Positions and relative strengths of components are shown by marks below the line.

Figure 7. The Mn II λ4206 line in HR 7361 (histogram). A single-line fit (dotted line) to the observed W_λ does not match well. Using the same hfs model as in Fig. 5 (dot–dash line) produces an improved fit.

Figure 5. The Mn II λ4206 line in HR 7775 (histogram). A single-line fit (dotted line) with the observed W_λ does not match well. Using a two-component (dashed line) or three-component (dot–dash line) hfs model (Table 5) provides increasingly better fits. Positions and relative strengths of components are shown by the marks below the line.

order to avoid an overly complicated multiple-component model, while fitting reasonably well the asymmetric profiles in all the sharp-lined stars studied. Again, the actual (but unknown) hfs is undoubtedly very much more complicated, with 16 components

($I = 5/2$, $J_u = J_l = 4$), some of which would be very weak. The approximation derived here permits reasonable-looking synthesis fits to all the stars in the sample.

Storey (private communication) has made available preliminary calculations of the detailed hyperfine structure of λ4206 of Mn II especially for the present investigation. The uncertainties in the 15-component structure obtained are considerable and further work is needed. However, if we allowed the derived pattern to have the largest width still consistent with our spectra of HR 7775 and 7361, the abundances derived (see Table 4) in the stars with the strongest lines would be reduced by a further 0.2 dex.

Without the hfs hypothesis, we can fit the λλ4206 and 4326 equivalent widths (in stars with strong Mn) only with an extremely high abundance (2–3 dex greater than that from the other lines of Mn II), and these synthetic profiles do not fit, as the line wings become too wide and the cores too shallow. Therefore, the hfs hypothesis solves the profile problem for both lines but does not completely eliminate the abundance discrepancy.
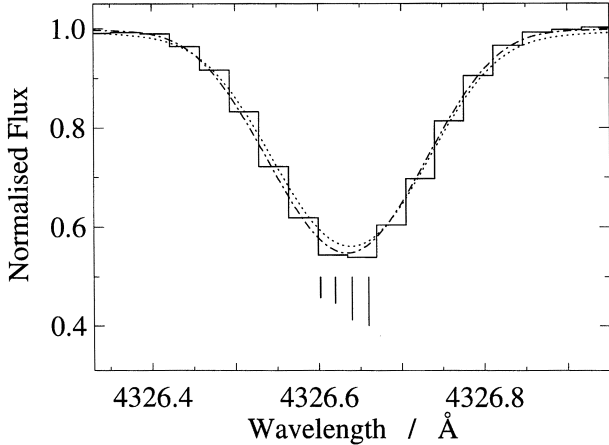
Figure 8. The Mn II λ4326 line in HR 7361 (histogram). A single-line fit (dotted line) does not match well. Using the same hfs model as in Fig. 6 (dot-dash line) produces an improved fit.

Table 5. Model hfs structures used for λλ4206 and 4326.

λ	log *gf*
4206.324	−2.040
4206.367	−2.040
4206.410	−2.040
4326.602	−2.078
4326.620	−1.975
4326.640	−1.763
4326.660	−1.710

The mean Mn II abundance (taken from the data in Table 2) is compared with the three-component results for λ4206 in Table 4 and Fig. 9, and with the four-component results for λ4326 in the same table and figure. As noted above, the trends in Fig. 9 show clearly that the simplified hfs models adopted here go a long way towards explaining the unexpected strengths of these lines, but do not entirely eliminate a discrepancy in derived abundance. The single exception to these trends is 33 Gem, which is treated in this work as a single star, but was suspected of being a double-lined spectroscopic binary by Hubrig & Launhardt (1993). As previously noted, the question of binarity is not yet resolved, although our spectra did have the same 'square' profiles observed by Hubrig & Launhardt.

Given the expectation that the hfs of these two lines should be very complicated, we believe that at least some of the residual trends of their abundance discrepancies versus mean abundance from other lines may be due to the numerous weak hfs components. Our preliminary model using Storey's predictions does not predict complete elimination of the residual discrepancies, although the effect is in the right direction. A laboratory study of the hfs in Mn II is urgently required to resolve these problems.

We also conducted an experiment to test the effect of systematic errors in microturbulence (see also the error discussion in Section 3.3): the results demonstrated that postulating substantially larger (1 km s^{-1}) microturbulence in HR 7361, a star with very strong

Mn II and a relatively low $v \sin i$, has only a small (−0.1 dex) effect on the derived abundance.

6 DISCUSSION

Almost 30 years ago, Aller (1970) first proposed that the observed overabundances of Mn in HgMn stars followed a positive temperature trend. Since then, her result has been confirmed and extended by, for example, Adelman (1989) and SD93, who showed that when a large enough sample of HgMn stars is observed, the trend displays an upper envelope. Our Mn abundance results confirm in remarkable detail those of SD93 (with improvements for the double-lined binary stars). In Fig. 10 the dashed line at $\log A = 5.39$ indicates the solar abundance of Mn (Anders & Grevesse 1989). For ν Cnc the visible-region data yielded only an upper limit, hence we plot for that star the UV-derived abundance of SD93, marked as a cross. The dotted line is the maximum photospheric abundance of Mn that can be supported in a homogeneous atmosphere by radiative acceleration (Alecian & Michaud 1981). We note the apparent remarkable agreement between the distribution of the highest abundances as a function of $T_{\rm eff}$ and the shape of the theoretical upper envelope. This is a more important confirmation of a prediction of diffusion theory than exact vertical agreement (SD93), because calculations by SD93 showed that the lower values of observed (or inferred) maximum abundances from homogeneous models could be interpreted as being due to Mn being stratified in relatively thin layers at $\tau_0 < 10^{-2}$. We also confirm the existence of a class of hot HgMn stars which exhibit only mild Mn enhancements and other anomalies as described by Cowley (1980), SD93 and Smith (1993).

The internal agreement of abundances in our results for Mn I and Mn II over a wide range of $T_{\rm eff}$ is remarkable. One might well have expected some effects of stratification or non-LTE on the ionization balance, but the LTE results presented here (based on the assumptions of homogeneous abundance distributions with optical depth) show a remarkable coherence between the results from neutral and singly ionized Mn, as well as between visible-region lines and UV resonance lines. In the absence of a detailed calculation, we cannot comment on possible non-LTE effects on equivalent widths other than to predict (on the basis of our results) that they ought not to be expected to be large. This expectation should be checked by a detailed calculation, which is beyond the scope of the present paper. It is possible that non-LTE or stratification effects (or a combination of both) are responsible for the remaining (0.3–0.4 dex) discrepancies between the hfs-affected lines λλ4206, 4326 and the other Mn II lines.

The fact that hfs must be having some sort of effect on many atomic species including the Mn II lines, and should therefore be taken into account in abundance analyses, was recognized by Booth & Blackwell (1983), but the present paper is the first abundance analysis of Mn II in HgMn stars that explicitly attempts to take this into account. As shown in our previous work on Ga (Dworetsky et al. 1998), these hfs effects can be dominant; here they have been shown to be enormous (2–3 dex) for certain strong lines. It is interesting that some Mn II lines appear to be relatively free of significant hfs broadening. Obviously, future work on abundance determinations should concentrate on lines like λ4478, which are evidently free of significant hfs curve-of-growth effects. However, while we have accounted for much of the abundance discrepancy to be found in analyses based on simple equivalent width calculations, we have not been able to account for all the deduced abundance differences between λλ4206, 4326 and the other weaker lines by using our ad hoc hfs models. We suspect that part of the remaining
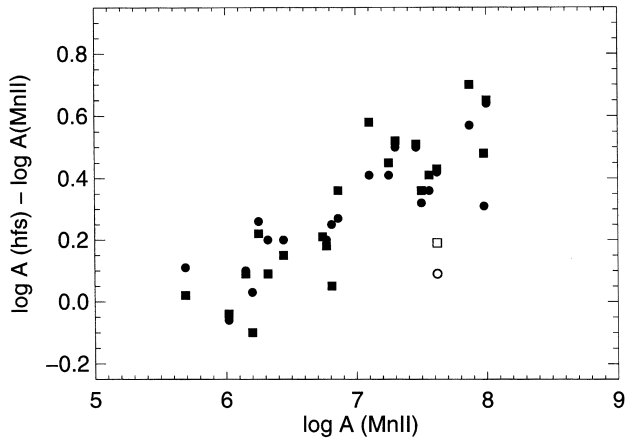
Figure 9. The residual abundance excess from the simplified model hfs versus mean Mn II abundance from the other visible-region lines: filled squares, λ4206; filled circles, λ4326; open symbols, 33 Gem (see text).
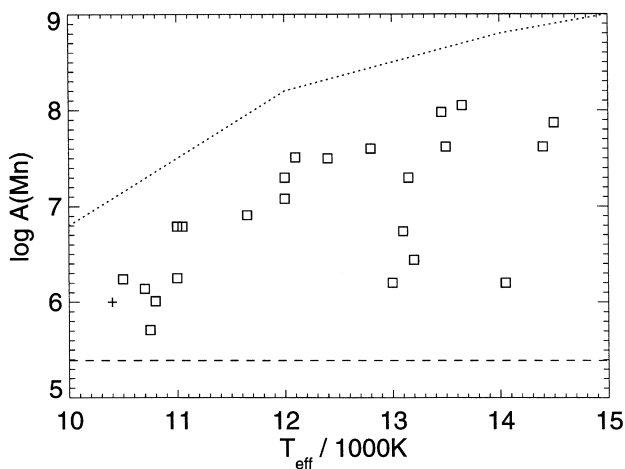

Figure 10. Mn abundance versus T_{eff}. Solar abundance is given by the dashed line. The dotted line indicates the maximum supportable abundance of Mn under the assumption of a homogeneous distribution with optical depth. The envelope would be lower if Mn were concentrated in a stratified layer high in the photosphere (SD93). The cross indicates *ν* Cnc, taken from the UV abundance.

discrepancies could be eliminated if a laboratory study of hfs in Mn II were to be made available through laboratory spectroscopy, and we urge our colleagues in that field to examine this interesting astrophysical problem.

7 CONCLUSIONS

We have measured the manganese abundance in 24 HgMn stars using a curve-of-growth technique, using six well-characterized Mn I and Mn II lines. A more detailed spectral synthesis analysis for a selection of stars confirms the accuracy of this simpler method when a few good unblended lines of moderate strength are used. The results agree well with the UV abundances of SD93 for all the isolated stars and some of the binaries. The remaining binary stars show a higher abundance in the visible region than the UV, which is to be expected, since SD93 did not account for binarity. The remarkably small scatter amongst the abundances derived for individual lines and the excellent

agreement with the UV results show that careful selection of a few well-characterized lines is a powerful tool for a quick and accurate abundance analysis. The similarity between the abundances derived for Mn I and Mn II may imply that we see very little in the way of non-LTE effects. The results support the comparison by SD93 of the predictions of diffusion theory by Alecian & Michaud (1981) with abundance trends for the upper envelope of abundances as a function of T_{eff}. This is another detailed prediction of the theory that has been confirmed observationally.

We have presented strong evidence that hyperfine structure is the cause of the widened line profiles and is mainly responsible for the line strength anomalies seen in Mn II λλ4326 and 4206, and we have shown that hfs can be a major source of systematic error if not taken into account in abundance analyses. The other Mn lines studied must have very much narrower hfs structures, to give such consistent results. We were able to derive crude ad hoc structures, but a laboratory study of hfs in Mn II is urgently needed if more precise results are to be obtained.

REFERENCES

Abt A., 1952, ApJ, 115, 119
Adelman S. J., 1989, MNRAS, 239, 487
Adelman S. J., 1992, MNRAS, 258, 167
Adelman S. J., Philip A. G. D., Adelman C. J., 1996, MNRAS, 282, 953
Alecian G., Michaud G., 1981, ApJ, 245, 226
Allen C. S., 1998, PhD thesis, Univ. London (http://www.ulo.ucl.ac.uk/ulocomms/80/index.html)
Aller M. F., 1970, A&A, 6, 67
Anders E., Grevesse N., 1989, Geochim. Cosmochim. Acta, 53, 197
Bohlender D. A., Dworetsky M. M., Jomaron C. M., 1998, ApJ, 504, 533
Booth A. J., Blackwell D. E., 1983, MNRAS, 204, 777
Castelli F., Gratton R. G., Kurucz R. L., 1997, A&A, 318, 841
Churchill C. W., 1995, Lick Obs. Tech. Rep. No. 74
Cowley C. R., 1980, PASP, 92, 159
Dworetsky M. M., Jomaron C. M., Smith C. A., 1998, A&A, 333, 665
ESA (European Space Agency), 1997, The Hipparcos and Tycho Catalogues, ESA SP-1200
Harman D. J., 1997, MSc Project Report, University College London
Heacox W. D., 1979, ApJS, 41, 675
Hubrig S., Launhardt R., 1993, in Dworetsky M. M., Castelli F., Faraggiana R., eds, ASP Conf. Ser. Vol. 44, Peculiar versus Normal Phenomena in A-Type and Related Stars. Astron. Soc. Pac., San Francisco, p. 350
Kurucz R. L., 1990, Trans. IAU, XXB, 168 (CD-ROM 23)
Kurucz R. L., 1993, ATLAS9 Stellar Atmosphere Programs and 2 km s^{-1} Grid (CD-ROM 13)

Kurucz R. L., Furenlid I., Brault J., Testerman L., 1984, Solar Flux Atlas from 296 nm to 1300 nm (NSO Atlas No 1)

Lanz T., 1995, in: Adelman S. J., Wiese W. L., eds, ASP Conf. Ser. Vol. 78, Astrophysical Applications of Powerful New Databases. Astron. Soc. Pac., San Francisco, p. 423

Martin G. A., Fuhr J. R., Wiese W. L., 1988 J. Phys. Chem. Ref. Data, 17, Suppl. 3, 1

Michaud G., 1970, ApJ, 160, 641

Michaud G., 1986, in Cowley C. R., Dworetsky M. M., Mégessier C., eds, Proc. IAU Colloq 90, Upper Main Sequence Stars with Anomalous Abundances. Reidel, Dordrecht p. 459

Misch A., 1997, User's Guide to the Hamilton Echelle Spectrometer (http://www.ucolick.org/~tony/instruments/hamspec/hamspec_index.html)

Ryabchikova T. A., Zakhorova L. A., Adelman S. A., 1996, MNRAS, 283, 1115

Smith K. C., 1992, PhD thesis, Univ. London

Smith K. C., 1993, A&A, 276, 393

Smith K. C., 1997, A&A, 319, 928

Smith K. C., Dworetsky M. M., 1988, in Adelman S. J., Lanz T., eds, Elemental Abundance Analyses. Institut d'Astronomie de l'Univ. de Lausanne, Switzerland p. 32

Smith K. C., Dworetsky M. M., 1993, A&A, 274, 335 (SD93)

Smith P. L., 1976, MNRAS, 177, 275

Valdes F., 1990, The IRAF APEXTRACT Package (ftp://iraf.tuc.noao.edu/iraf/docs/apex.ps)

Vauclair S., Vauclair G., 1982, ARA&A, 20, 37

Vogt S., 1987, PASP, 99, 1214

Warner B., 1967a, Mem. R. Astron. Soc., 70, 165

Warner B., 1967b, MNRAS, 136, 381

This paper has been typeset from a T_EX/L^{A}T$_E$X file prepared by the author.